Research Article | Vol. 9, No. 11 | 1 Nov 2018 | BIOMEDICAL OPTICS EXPRESS 5703
Biomedical Optics EXPRESS

Anti-cancer effect of bee venom on human MDA-MB-231 breast cancer cells using Raman spectroscopy

GYEONG BOK JUNG,[1,7] JEONG-EUN HUH,[2,7] HYO-JUNG LEE,[3] DOHYUN KIM,[4] GI-JA LEE,[5,8] HUN-KUK PARK,[5] AND JAE-DONG LEE[6,9]

[1]*Department of Physics Education, Chosun University, Gwangju, 61452, South Korea*
[2]*East–West Bone & Joint Research Institute, Kyung Hee University, 149, Sangil-dong, Gangdong-gu, Seoul, South Korea*
[3]*College of Korean Medicine, Kyung Hee University, 1, Hoegi-dong, Dongdaemun-gu, Seoul, South Korea*
[4]*Department of Industrial and Management Engineering, Myongji University, Gyeonggi-do 17058, South Korea*
[5]*Department of Biomedical Engineering College of Medicine, Kyung Hee University, Seoul 02447, South Korea*
[6]*Department of Acupuncture and Moxibustion, College of Korean Medicine, Kyung Hee University, 1, Hoegi-dong, Dongdaemun-gu, Seoul, South Korea*
[7]*These authors contributed equally to this work.*
[8]*gjlee@khu.ac.kr*
[9]*ljdacu@khmc.or.kr*

Abstract: We demonstrated the apoptotic effect of bee venom (BV) on human MDA-MB-231 breast cancer cells using Raman spectroscopy and principal component analysis (PCA). Biochemical changes in cancer cells were monitored following BV treatment; the results for different concentrations and treatment durations differed markedly. Significantly decreased Raman vibrations for DNA and proteins were observed for cells treated with 3.0 μg/mL BV for 48 h compared with those of control cells. These results suggest denaturation and degradation of proteins and DNA fragmentation (all cell death-related processes). The Raman spectroscopy results agreed with those of atomic force microscopy and conventional biological tests such as viability, TUNEL, and western blot assays. Therefore, Raman spectroscopy, with PCA, provides a noninvasive, label-free tool for assessment of cellular changes on the anti-cancer effect of BV.

1. Introduction

Bee venom (BV) extracted from honey bees is commonly used in Korean medicine to treat diseases, including pain, arthritis, tumor, and skin diseases [1–3]. It is composed of a complex mixture of biologically active peptides, including melittin (a major component of BV), apamin, adolapin, mast-cell-degranulating (MCD) peptide; enzymes (phospholipase A2, and hyaluronidase), and non-peptide components (histamine, dopamine, and norepinephrine), which have a variety of pharmaceutical properties [2–5]. Recent studies have shown that BV has anti-cancer effects, including induction of apoptosis and inhibition of proliferation in various cancer cells, such as prostate, breast, lung, liver, ovarian, and bladder [3,6–9]. The efficacy of BV appears to be due to the synergistic effect and selective cytotoxicity of melittin, and this anti-cancer peptide might be a better choice than the native form of BV [10,11].

The interaction of anti-cancer agents with the affected cells is considered to be very important for the selection and optimization of a drug to attain the most effective cancer treatment. It is well known that the function of an anti-cancer agent is to induce apoptosis of

#345244 https://doi.org/10.1364/BOE.9.005703
Journal © 2018 Received 6 Sep 2018; revised 16 Oct 2018; accepted 16 Oct 2018; published 25 Oct 2018

Biomedical Optics EXPRESS

the target cancer cells. Apoptosis is characterized by cellular morphological changes, such as shrinkage, membrane blebbing, DNA cleavage, caspase activation, and mitochondrial dysfunction [12–14].

Assays for apoptosis, such as MTT and western blot that measure enzymatic activity and protein synthesis as endpoints and are associated with cell viability, have been investigated for chemosensitivity testing [15]. These assays are invasive, destructive, time-consuming, labor-intensive, and involve complicated procedures. Furthermore, it requires large amounts of material, while the product yield is low. The dynamics of the interactions cannot be examined directly with these assays as the introduction of fluorescent labels during measurement can change the biological conditions. Therefore, a non-invasive, label-free analytical technique is needed for the real-time monitoring of live cells.

Raman spectroscopy is a non-invasive and rapid detection technique that requires no sample labeling prior to analysis [16–19]. Thus, this technique is being explored extensively for the analysis of biological systems. Raman spectroscopy provides quantitative information about the molecular structure, chemical composition, and molecular interactions within the cells, with high sensitivity and selectivity. The intracellular information about nucleic acids, proteins, lipids, and other components can be explored using variations in spectral shape or intensity [20–23]. Raman spectroscopy has been applied for the analysis of the effect of external agents on the cells, causing specific time-dependent biochemical changes associated with the process of cell death [24–29]. Notingher *et al*. used Raman spectroscopy to measure the time-dependent molecular changes in cells during apoptosis [28]. Byrne *et al*. evaluated the effect of the chemotherapeutic drug Actinomycin D in A549 lung cancer cell line using Raman spectroscopy [30]. However, the anti-cancer effect of BV on breast cancer cells has not been evaluated by Raman spectroscopy.

In this study, we investigated the biochemical changes at the molecular level in human MDA-MB-231 breast cancer cells using Raman spectroscopy following exposure to BV. In addition, we examined the correlation between the Raman data and the results from conventional cytotoxicity assays and apoptotic DNA damage. We also investigated the morphological characteristics of MDA-MB-231 cells following BV treatment using atomic force microscopy (AFM).

2. Materials and methods

2.1 Cell culture and treatment

The MDA-MB-231 human breast cancer cells were obtained from the American Type Culture Collection (Manassas, VA, USA). The cells were cultured in Dulbecco's modified Eagle medium (DMEM) supplemented with 10% fetal bovine serum (FBS) and antibiotics, in a humidified atmosphere containing 5% CO_2 and 95% air at 37°C. Human peripheral blood mononuclear lymphocytes (PBMLs) were isolated from the blood of the donors by Ficoll-hypaque gradient centrifugation. Blood was layered onto high-density Ficoll-Hypaque medium (Ficoll 400, GE Healthcare Life Sciences) at density 1.114 g/mL and centrifuged at 600 × g for 30 min at room temperature. PBMLs resolved into two distinct bands, the upper containing PBMC and the lower containing neutrophils. PBMLs were harvested and washed three times in phosphate buffered saline (PBS) [31]. For AFM and Raman spectroscopic analysis, the cells were cultured on gold-coated glass (5 mm × 5 mm) and incubated for 24 h. The cells were treated with bee venom (Sigma-Aldrich, MO, USA: The composition of the BV was as follows: 50-55% melittin, 2.5-3% apamin, 2-3% MCD peptide, 12% PLA_2, 1% lyso-PLA, 0.5-1% histidine, 1.5-2% hyaluronidase, 2% amine and 10-17% other, including protease inhibitor, glucosidase, invertase, acid phosphomonoesterase, dopamine, nonepinephrine, with > 99.5% purity) and further incubated for 24 h. The cells were washed twice with PBS and fixed in 4% paraformaldehyde in PBS for 20 min at 4°C. After fixation, the gold-coated substrate was briefly washed with PBS and deionized water and air-dried.

Biomedical Optics EXPRESS

2.2 Viability assay

The cells were seeded (2×10^5 cells per well) in 96 well plates, subsequently the subconfluent cells were treated with BV (0.7, 1.5, 3.0, 6.0, and 12.5 µg/mL) or vehicle (saline) for 12 h, 24 h, 48 h and 72 h. After treatment, cell viability was measured using the Cell Counting Kit-8 (CCK-8) according to the manufacturer's instructions. Briefly, the CCK-8 solution (10 µL per 100 µL of medium in each well) was added, the plates were incubated at 37°C for 1 h, and the absorbance of each well was read at 450 nm using a microplate reader.

2.3 TUNEL assay

The Apoptosis Detection System developed by Promega was used according to the supplier's protocol. Briefly, after treatment with 3.0 µg/mL of BV for 12 h, 24 h and 48 h, the cells were washed twice with PBS, and 5 mL of 1% ice-cold paraformaldehyde was added for 20 min. The cells were incubated for 1 h at 37°C in the dark in 50 µL of equilibration buffer containing fluorescein-12-dUTP in the presence of terminal deoxynucleotidyl transferase to label 3′-OH ends of fragmented DNA. The reaction was stopped by adding 1 mL of 20 mM EDTA, and the cells were washed with PBS containing 0.1% Triton X-100 and 5.0 µg/mL of bovine serum albumin (BSA). The cells were stained with a mixture of 5.0 µg/mL of propidium iodide (PI) and 250 µg of RNase A, incubated at room temperature in the dark for 30 min before analysis by fluorescence microscopy (Axiovert S 100, Zeiss, USA) and captured using an Axiocam MRc5 CCD camera (Carl Zeiss, Germany) at × 200 magnification.

2.4 Flowcytometry analysis

Surface exposure of phosphatidylserine (PS) by apoptotic cells was measured by flow cytometer by adding annexin V- V-FITC (Becton Dickinson, USA) according to the manufacturer's specifications (Annexin V Detection Kit), and stained simultaneously with PI. Samples were analyzed on a FACSort flow cytometer using standard Lysis II software (Becton Dickinson, USA). Excitation was set at 488 nm, and the emission filters used were 515-545 nm (green, FITC) and 600 nm (red, PI).

2.5 Western blot analysis

Proteins were extracted from MDA-MB-231 cells treated with BV (0.7, 1.5, 3.0 µg/mL) or vehicle (saline) for 12 h, 24 h, and 48 h. The cells were lysed with protein lysis buffer, and the protein concentrations were determined by Bradford protein assay. Determination of microgram quantities of protein in the Bradford Coomassie brilliant blue assay (Bio-Rad, Laboratories, Inc., CA, USA) is accomplished by measurement of absorbance at 590 nm) [32]. The proteins were separated using 12% SDS-PAGE, and then transferred to Hybond-ECL [enhanced chemiluminescence] membranes (Amersham, Little Chalfont, Buckinghamshire, UK). The membranes were blocked with 6% non-fat milk dissolved in TBST buffer (10 mM Tris-Cl [pH 8.0], 150 mM NaCl, 0.05% Tween 20). The blots were then probed with various rabbit polyclonal antibodies for PARP, Caspase-8, Caspase-9, Caspase-3 (0.5 µg/mL; Cell Signaling Tech., MA, USA), β-actin and or non-immune mouse IgG (0.5 µg/mL; Sigma-Aldrich Co, MO, USA) diluted 1:1,000 in Tris-buffered saline at 4°C overnight; and then incubated with 1:2,000 dilutions of goat anti-rabbit IgG secondary antibody coupled with horseradish peroxidase. The membranes were washed with TBST between each treatment. The blots were developed using the ECL method (GE Healthcare).

2.6 AFM measurement

Non-contact mode AFM images were obtained using a NANOstation II (Surface Imaging Systems, Herzogenrath, Germany) equipped with a 42.5 µm XY/4 µm Z scanner and a Zeiss optical microscope (Epiplan 50). AFM was performed on an active vibration isolation table

Biomedical Optics EXPRESS

(TS-150, S.I.S., Herzogenrath, Germany) inside a passive vibration isolation table (Pucotech, Seoul, Korea) to eliminate external noise. Non-contact mode AFM imaging was performed at room temperature using a silicon cantilever with aluminum reflex coating (Budget Sensor, Bulgaria). The material properties and dimensions of the probe used in this study was as follows: resonance frequency, 190 kHz; force constant, 48 N/m; cantilever length, 225 μm; cantilever width, 38 μm; cantilever thickness, 7 μm; tip radius, < 10 nm; and tip height, 17 μm. The MDA-MB-231 cells were scanned at a resolution of 512 × 512 pixels with a scan rate of 0.6 lines/s.

2.7 Raman spectroscopy

For the Raman spectroscopic measurements, we used gold-coated substrate. A thin 10 nm, Cr layer followed by a 50 nm gold layer were e-beam evaporated on the glass substrate. The Cr layer was included to increase the adhesion between the gold film and the glass substrate. This substrate was minimized spectral contributions from the sample substrate such as glass and enhanced the Raman signal compared to that. Pure metals are known to have no Raman spectral features and very low background signal. For the isolated single cells, the relative position of the laser can potentially affect the spectrum. Thus for all the isolated single cells used, the position of the spot was retained the same in relation to the cell, which the Raman spectra were obtained centrally over the nucleus of the cells when visible. At least ten individual cells were selected from each cell-group for measurement. Raman spectra were acquired using the SENTERRA confocal Raman system (Bruker Optics Inc., Billerica, MA, USA) equipped with a 785-nm diode laser source (100 mW before objective) and a resolution of 3 cm^{-1}. A 100x air objective (MPLN N.A. 0.9, Olympus), which produces a laser spot size of ~1 μm was used to collect Raman signals and focus the laser on a single cell. The raw spectra were loaded into OPUS software (Bruker Optics Inc., Billerica, MA, USA) to remove cosmic rays manually and subtract the autofluorescence background from every sample spectrum. Raman spectral acquisition and pre-processing of preliminary data, such as baseline subtraction, smoothing, normalization and spectrum analysis were carried out using OPUS software. An automated algorithm for autofluorescence background removal was applied to the measured data to extract pure sample Raman spectra. Baseline correction was performed using the rubber-band method, which was used to stretch between the spectrums endpoints. The baseline-corrected Raman spectra were normalized using the vector normalization method. All Raman measurements were recorded with an accumulation time of 60 s in the 600-1750 cm^{-1} range. The Raman spectra of the cells were calculated as the average of ten measured samples.

2.8 Multivariate analysis

Principal component analysis (PCA) was used for statistical analysis. It is one of the multivariate statistical techniques for reducing high-dimensional data to low-dimensional data. The goal of the PCA is to find the fewest uncorrelated variables, called the principal components (PCs), to account for the maximum variance of the data. As a result, the first principal component has the largest variance possible, and each subsequent principal component has the highest possible variance in orthogonal position with the preceding components. For PCA, MATLAB's statistics and machine learning toolbox was used. The data sets used for PCA, include Raman spectral data sets based on various concentrations and time periods. Raman spectral data based on various concentrations consist of 40 observations; 10 observations for each concentration (i.e., 0, 0.7, 1.5, and 3.0 μg/mL). Data based on various time periods have a total of 40 observations; 10 observations for each time period (i.e., 0, 12, 24, and 48 h) Raman intensities measured at 2301 frequencies (600–1750 cm^{-1}) were used as original variables for data analysis. From the PCA-based spectrum data sets, the principal component scores and loadings for each PC were calculated. The three PCs obtained

Biomedical Optics EXPRESS

account for about 82.2% (concentration data), and 74.9% (time period data) of the total variance in all the variables.

2.9 Statistical analysis

Values are expressed as means ± standard error of the mean (S.E.M). Student a*r*t tests were performed for comparing 2 groups, and differences among groups were analyzed by one-way ANOVA. The statistical analyses were performed using the Prism 5.0 program. Differences were considered statistically significant at $p < 0.05$.

3. Results and discussion

3.1 Cytotoxic effect of BV on MDA-MB-231 cells and PBMLs cells

To evaluate the cytotoxic effect of BV on the human MDA-MB-231 breast cancer cells and normal cells, cell viability was determined using the CCK-8 assay. Bee venom significantly inhibited the proliferation of MDA-MB-231 cells; IC_{50} values of 5.2, 4.5, 3.0, and 2.8 μg/mL were obtained for 12, 24, 48, and 72 h incubation post-treatment, respectively, as shown in Fig. 1(A). To differentiate between the susceptibilities of cancer cells and normal cells, we explored the effects of BV in PBMLs. As shown in Fig. 1(B), BV did not show any significant cytotoxic effect on PBMLs till doses of 12.5 μg/mL and 72 h incubation.

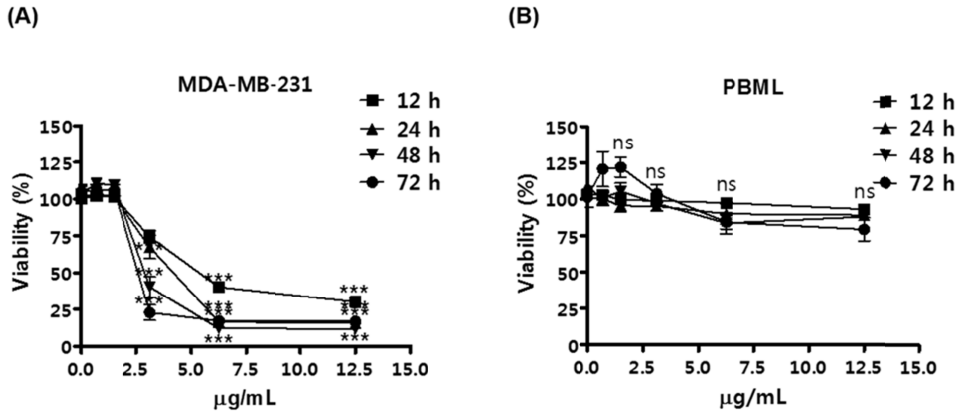

Fig. 1. Effects of bee venom on the viability of human MDA-MB-231 breast cancer cells and peripheral blood mononuclear lymphocytes (PBMLs). Cells were seeded in 96-well plates at a density of 2×10^5 cells/well and allowed to attach for 12 h in growth medium. MDA-MB-231 cells (A) and PBMLs (B) were then treated with various doses of BV (0.7, 1.5, 3.0, 6.0 and 12.5 μg/mL) for 12, 24, 48, and 72 h. Cell viability was assessed using Cell Counting Kit-8. Values are expressed as means ± S.E.M. of 3 independent experiments. ***$p < 0.001$ compared with control; n.s., nonsignificant difference compared with control.

Biomedical Optics EXPRESS

3.2 BV-induced apoptotic cell death in human MDA-MB-231 cells

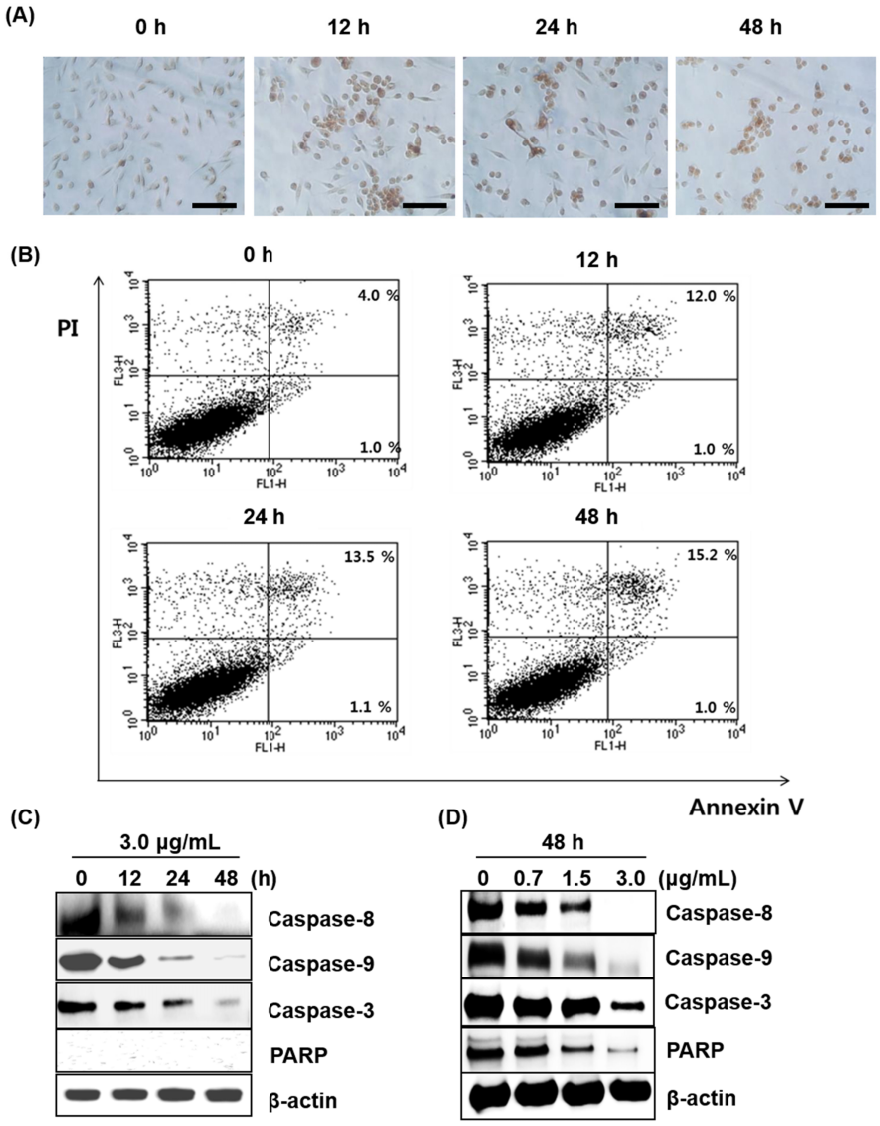

Fig. 2. Effect of bee venom on apoptotic cell death of human MDA-MB-231 breast cancer cells. (A) Cells treated with BV (3.0 μg/mL) for 12, 24 and 48 h and apoptotic cell death was determined by TUNEL staining. The staining of fragmented DNA and cell morphology was analyzed by fluorescence microscopy. Scale bars represent 100 μm. (B) Cells stained with annexin V-FITC and propidium iodide for 5–15 min in the dark and analyzed by flow cytometer. (C) The relative expression level of caspase-8, -9, -3, PARP upon exposure to 3.0 μg/mL BV at the indicated time points was measured using western blot analysis, and normalized using β-actin. Equal amounts of the total protein extracts of MDA-MB-231 cells were separated by 12% SDS-polyacrylamide gel electrophoresis and transferred onto Hybond-ECL membranes. The membranes were probed with the antibodies against caspase-8, -9, -3, PARP and β-actin. Proteins were visualized using the ECL detection system. (D) Western blot analysis showing the expression of caspase-8, -9, -3, PARP in response to different concentrations of BV for 48 h.

Biomedical Optics EXPRESS

To identify the apoptotic effect of BV in MDA-MB-231 cells, we performed the TUNEL assay. We observed many TUNEL-positive cells with small, dense, and fragmented morphology emitting yellow fluorescence, whereas the PI stained nucleus in the control cells exhibited round morphology and emitted red fluorescence as shown in Fig. 2(A). To confirm the mode of BV-induced cell death, we stained the MDA-MB-231 cells with annexin V/PI for 12 h, 24 h and 48 h after exposure to 3.0 μg/mL of BV, and analyzed by flow cytometry. Figure 2(B) shows a time-dependent increase in the number of annexin V-positive cells, such as 12.0%, 13.3%, and 15.2% for 12 h, 24 h and 48 h of exposure, respectively, was observed, suggesting that BV initiated apoptosis in this cell population and it did not increase the number of necrotic cells double-stained with annexin V/PI. Caspases are believed to play a central role in the apoptotic signaling pathway. Therefore, we evaluated the expression of caspase-8, –9 and –3 in MDA-MB-231 cells following treatment with 3.0 μg/mL BV for 12 h, 24 h and 48 h. Interestingly, we observed that BV inhibits the protein level of caspase-8, –9 and –3 of MDA-MB-231 cells in a time-dependent manner (Fig. 2(C)). Also, BV caused the proteolytic cleavage of PARP, determined by the disappearance of the full-length 116 kDa protein of MDA-MB-231 cells (Fig. 2(C)). Bee venom dose-dependently reduced the expression level of caspase-8, –9 and –3 and PARP of MDA-MB-231 cells (Fig. 2(D)).

3.3 Morphological changes in MDA-MB231 cells by BV treatment

We performed AFM measurement to observe the morphological changes in MDA-MB-231 cells following bee venom treatment. Figure 3 shows representative AFM topography images (40×40 μm^2) taken from fixed MDA-MB-231 cells that were treated with 0, 0.7, 1.5, and 3.0 μg/mL BV for 48 h (Fig. 3(A)), and 3.0 μg/mL BV for 0, 12, 24, and 48 h (Fig. 3(B)). The control cells had a regular spindle-like shape and the nuclei were elliptical and plump [33], and the cell surface seemed relatively smooth. Even after the cells were treated with 0.7 μg/mL of BV for 48 h, the morphology of the MDA-MB-231 cells did not change. However, when the cells were treated with 1.5 μg/mL of BV for 48 h, the surface around nuclei became a little rougher than that of the control cells. As the concentration of BV increased to 3.0 μg/mL, the cells changed greatly in size and shape; the cells shrunk and became round in shape. In addition, the cell membrane seemed to be rough due to protrusions and holes. And the change in surface roughness might be attributed to the damaged cell membranes by BV. Then, the time-dependent changes in MDA-MB-231 cells at 3.0 μg/mL of BV were examined (Fig. 3(B)). A little change in cell morphology was observed after 12 h of treatment. The cell seemed deformed after 24 h treatment, for example, the cell tails shrank a little. Over the course of 48 h, the cell morphology changed greatly in size and shape, and the tail also disappeared. Our previous study reported that the toxic effects of sodium lauryl sulfate (SLS) not only changed the spindle-like shape of L929 cells into a round shape, but also made the cell surface rough [34]. Therefore, the morphological changes in MDA-MB-231 cells might be attributed to the apoptotic cell death caused by BV.

Biomedical Optics EXPRESS

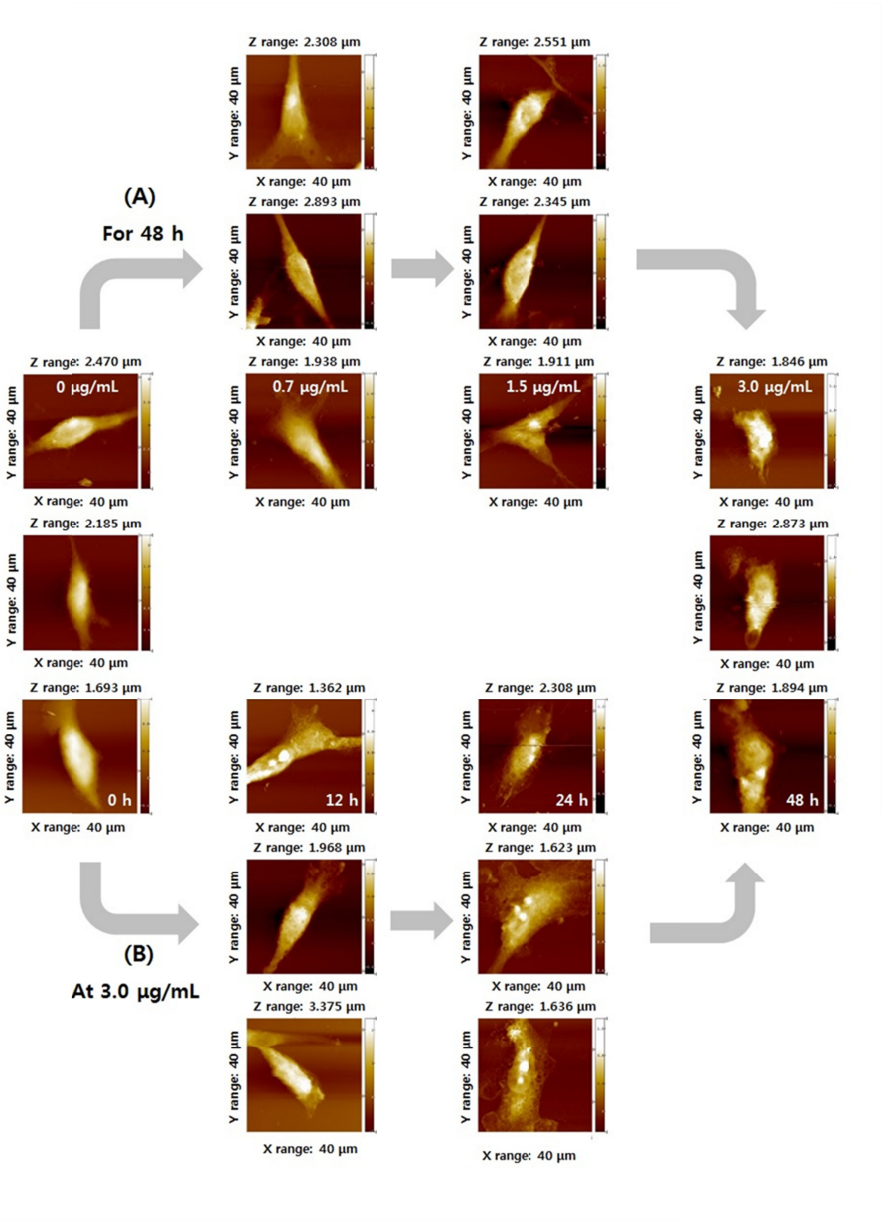

Fig. 3. Representative AFM topography images of fixed human MDA-MB-231 breast cancer cells treated with (A) 0, 0.7, 1.5, and 3.0 µg/mL of BV for 48 h and (B) 3.0 µg/mL of BV for 0, 12, 24, and 48 h.

Biomedical Optics EXPRESS

3.4 BV induces biochemical changes in MDA-MB-231 cells

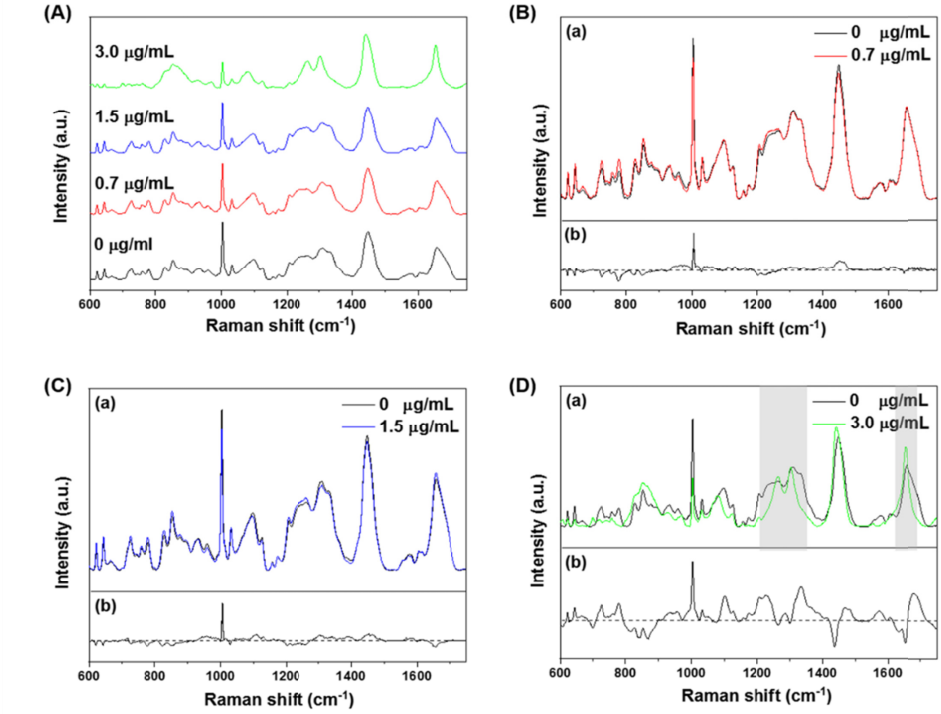

Fig. 4. Concentration-dependent Raman spectra of MDA-MB-231 cells treated with BV. (A) Averaged spectra for control and BV-treated cells; (B-D) (a) Overlaid spectra of control and BV-treated cells, (b) spectral differences between control and cells treated with BV: (B) 0.7 μg/mL, (C) 1.5 μg/mL, (D) 3.0 μg/mL.

The concentration-dependent (0, 0.7, 1.5, and 3.0 μg/mL) responses of the averaged Raman spectra of MDA-MB-231 cells after 48 h of BV treatment are shown in Fig. 4(A). They exhibited the characteristic vibrational bands for nucleic acids, proteins, and lipids (Table 1), which were similar to the previous Raman spectra for other cell types [19,35–42]. The prominent Raman bands at 853, 1003, 1032, 1265, and 1658 cm^{-1} belong to proteins. The band at 853 cm^{-1} was assigned to tyrosine, and the sharp band at 1003 cm^{-1} corresponded to the phenylalanine ring stretching. The 1032 cm^{-1} peak represented the vibrations of phenylalanine in plane CH bending. The broad bands at 1230-1320 represented amide III. The strong band at 1658 cm^{-1} represented amide I (α-helix) band of protein and the C = C stretching band of lipid. The band at 725 cm^{-1} is assigned to the adenine band of DNA, and the band at 779 cm^{-1} corresponded to the ring breathing mode of the DNA bases cytosine and thymine and the RNA base uracil. The 1098 cm^{-1} peak represented the vibrations of phosphodioxy groups (PO_2^-) in the DNA/RNA backbones. The strong band at 1449 cm-1 (CH deformations) was attributed to nucleic acid, proteins, and lipids. For a clear distinction between the spectral profiles, the BV-treated spectra were subtracted from the control spectra (Fig. 4(B-D)). An insignificant difference was observed between the Raman spectra of the control and that of the 0.7 μg/mL (Fig. 4(B)) and 1.5 μg/mL (Fig. 4(C)) of BV-treated cells.

Biomedical Optics EXPRESS

Table 1. Peak assignment of Raman spectra for human MDA-MB-231 breast cancer cell [19,35–42]

Peak (cm^{-1})	Assignment[a]			
	DNA/RNA	Proteins	Lipids	Carbohydrates
621		C-C twist. Phe		
643		C-C twist. Tyr		
665	G, T			
725	A			
758		Ring br. Trp		
779	U, C, T ring br.			
828	O-P-O asym. str.	Ring br. Tyr		
853		Ring br. Tyr		
878		C-C-N^+ sym. Str.	C-O-C ring	
932	C-C bk str. α-helix		C-O-C glycos	
1003	Sym. Ring br. Phe			
1032	C-H in-plane Phe			
1098	PO_2^- str.	Chain C-C str.	C-O, C-C str.	
1124		C-C str.		
1156	C-C/ C-N str.			
1173	C-H Tyr, Phe			
1207	C-C_6H_5 str. Phe, Trp			
1265	Amide III, α-helix			
1310	CH_3CH_2 twist.			
1449	G, A	CH def	CH def	
1576	G, A			
1605	C = C Phe, Tyr			
1658	Amide I, α-helix	C = C str.		

[a]Abbreviations: A, adenine; U, uracil; G, guanine, C, dytosine; T, thymine,; Phe, phenylalanine; Tyr, tyrosine; Trp, tryptophan; br, breathing; bk,backbone; def, deformation vibration; str, stretching; sym, symmetric; asym, asymmetric; tw, twist.

However, the most dramatic cellular changes in the MDA-MB-231 cells, associated with DNA, proteins, and lipids, were observed upon treatment with 3.0 μg/mL of BV (Fig. 4(D)). The major spectral differences were in the peaks associated with proteins (phenylalanine at 1003 cm^{-1}, 1032 cm^{-1}, amide III at 1230-1320 cm^{-1} and amide I at 1658 cm^{-1}), nucleic acids (U, C, and T at 779 cm^{-1}, and PO_2^- stretching at 1098 cm^{-1}), and lipid (C-H deformation at 1449 cm^{-1} and C = C stretching 1658 cm^{-1}). The magnitude of Raman intensity at 1003 cm^{-1}, 1032 cm^{-1}, corresponding to proteins, showed a decrease, which is due to the degradation of proteins as a related of cell death. Amide III (1230-1320 cm^{-1}) and amide I (1600-1700 cm^{-1})

Biomedical Optics EXPRESS

are the basic components of the protein structure, and also extremely sensitive to changes in the structure of the protein. As shown in Fig. 4(D), the amide III and amide I band widths in the BV-treated cells were narrower, compared to that of the control (gray color), which indicates the presence of a mixture of conformations, reflecting a difference in their protein secondary structure. The amide III band originates from the N-H in-plane deformation at 1276 cm^{-1}, coupled to the C-N stretching mode at 1243 cm^{-1} [43–45]. The amide I mode is a property of the peptide group, including the C = O stretching vibration with minor contributions from C-N and N-H motions [46–48]. Since the C = O stretching is differently involved in secondary structure elements via hydrogen bonds to the peptide N-H group, the band position correlates with different protein conformations. Thus, amide III and amide I bands are superimposed to get a multitude of single bands at different wavenumbers, which can be resolved in multiple components and attributed to different secondary structures [49–51]. Moreover, the 3.0 µg/mL BV-treated MDA-MB-231 cells showed a shift from 1449 cm^{-1} to 1443 cm^{-1}, and 1658 cm^{-1} to 1654 cm^{-1}. These Raman bands are frequently used to assign secondary structure to the proteins, and the shifts observed in these bands can be used as Raman markers for the conformational changes in the associated proteins as a result of the action of the BV. The band at 1098 cm^{-1} is considered as an internal standard for DNA content. As can be seen in Fig. 4(D), the intensity of the peak at 1098 cm^{-1} decreased in 3.0 µg/mL BV-treated cells in comparison to the control, suggesting changes in the DNA content due to drug intercalation. This observation is also supported by a similar variation observed in the guanine band at 725, and 779 cm^{-1}. These changes indicated nuclear DNA fragmentation as a result of apoptosis. Therefore, these bands can be considered as Raman signature for DNA intervention. It was previously reported that decrease in the Raman intensity was related to the degradation and conformational changes of proteins and DNA fragmentation, which correlated with cell death [19,21]. The intensity of the 1449 cm^{-1} (C-H deformation) and 1658 cm^{-1} (C = C stretching) bands increased the lipid-related Raman signal, indicating the presence of intracellular vesicles. This behavior is consistent with the formation of the lipid vesicles at the cell surface as well as blebbing of the cell membrane during apoptosis [52,53]. A similar increase in these bands was reported previously after the MDA-MB-231 cells were exposed to etoposide, an anti-cancer agent, resulting in apoptotic cell death [28].

To investigate the correlation between the time dynamics of the identified apoptotic molecular events, Raman spectra of the MDA-MB-231 cells treated with 3.0 µg/mL BV were determined 0, 12, 24, and 48 h post-treatment as shown in Fig. 5(A). For a clear distinction between the spectral profiles, the BV- treated spectra were subtracted from the control (0 h) spectra (Fig. 5(B-D)). The changes in Raman spectra were insignificant at 12 and 24 h, whereas they demonstrated dramatic cellular and molecular changes at 48 h. After 48 h, a decrease in the magnitude of Raman intensity was observed at 1003 and 1032 cm^{-1} (belonging to protein), and for the bands at 725, 779, and 1098 cm^{-1} (assigned to DNA). The intensity of the bands at 1449 and 1658 cm^{-1} reflected an increase in lipid-related Raman signal. As mentioned above, these results might indicate protein degradation, nuclear DNA fragmentation, and presence of intracellular vesicles leading to apoptotic cell death.

Biomedical Optics EXPRESS

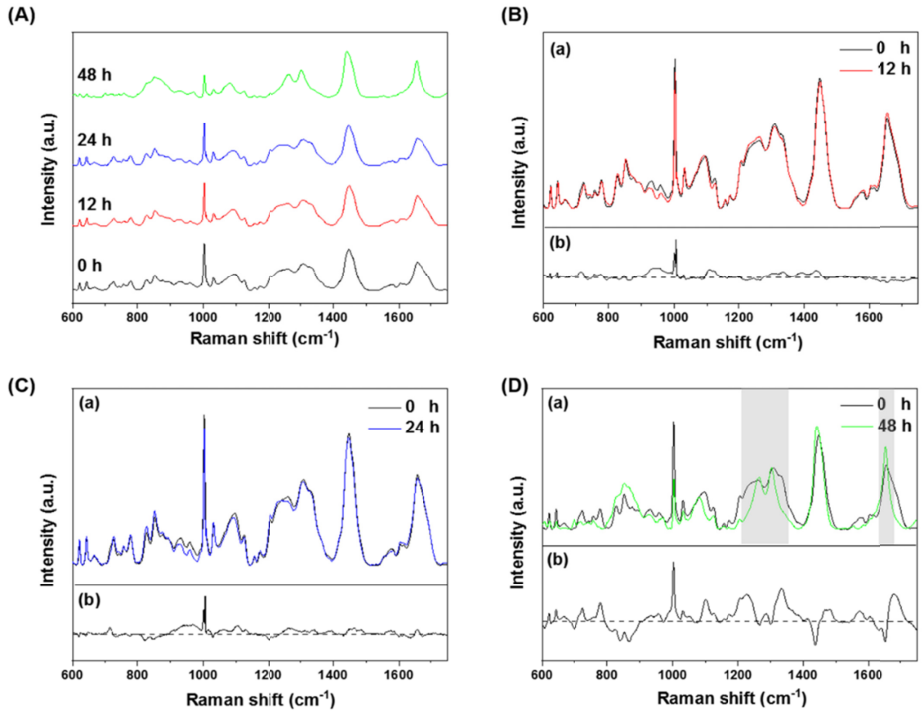

Fig. 5. Time-dependent Raman spectra of MDA-MB-231 cells treated with 3.0 μg/mL of BV. (A) Averaged spectra for control and BV-treated cells; (B-D) (a) Overlaid spectra of control and BV-treated cells, (b) spectral differences between control and cells treated with BV: (B) 12 h, (C) 24 h, (D) 48 h.

For a detailed analysis of the changes in Raman spectral features after exposure to BV, we employed PCA analysis. First, PCA was applied to Raman spectral data to distinguish between the different concentrations and then three PC scores, for each observation, are plotted in three dimensions. Figure 6(A) shows the plots of PC scores for 40 observations and loadings for 2301 variables. PC1 showed a clear distinction between 3.0 μg/mL of BV treatment and the other concentrations (0, 0.7, and 1.5 μg/mL), which showed a considerable overlap in the 3D plot. The PCA analysis validates all the results obtained for 3.0 μg/mL of BV treatment. Additionally, the loading plot showed the relationship between the original variables and the selected principal components, and the intensity plot demonstrated the average intensities of the observations for each concentration, and a total of 2301 variables. The representative Raman spectral peaks that play a major role in PC1 to PC3 are summarized in Fig. 6(B). Notably, the frequencies near 1003, 1334, 1437 and 1679 contribute significantly to PC1, which clearly differentiates the observations for 3.0 μg/mL and the observations for the other concentrations of BV.

Biomedical Optics EXPRESS

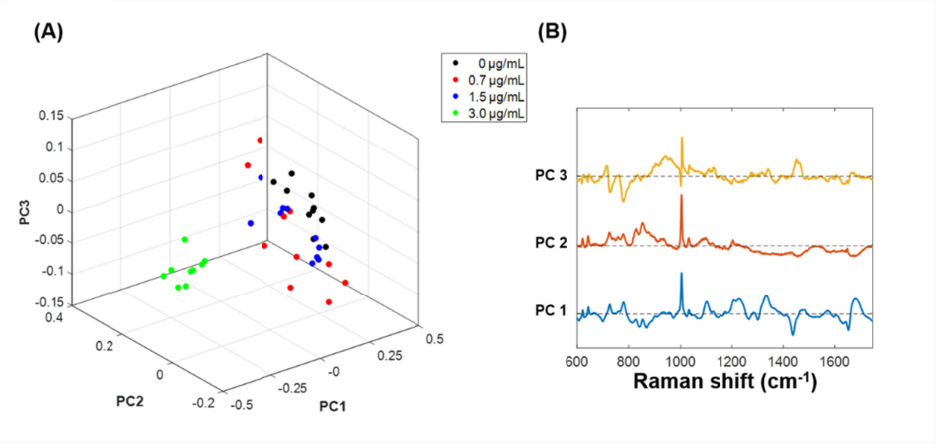

Fig. 6. Score plot and Loading plot for the Raman spectral data at the selected BV concentrations. (A) Score plot reveals the projection of the data onto the PCs in three dimensions for the Raman spectral data. (B) Loading plot highlights the important frequencies which contribute to each PC for the Raman spectral data.

A three-dimensional plot of time-dependent Raman spectra was also constructed with the three sets of scores (PC1 vs PC2 vs PC3) as shown in Fig. 7(A). Principal component analysis demonstrated an analytical grouping of the spectra at all time points. Especially, the PC1 vs PC2 plot showed clear differences between 12 h of treatment and the other time points (24 h and 48 h). Thus, different combinations of PC1, PC2 and PC3 can distinguish between the observations at different time points. Loading plots of PC1, PC2, and PC3 that lead to delineation between the control and BV-treated groups are presented in Fig. 7(B). The loading of PC1 is dominated by 1003, 1334, 1437, and 1679 cm^{-1}, similar to the case of BV concentration. In the loading of PC2 and PC3, the main peak features correspond to 851, 1003 cm^{-1} and 1006 and 1438 cm^{-1}, respectively. The results obtained from Raman spectroscopy, combined with PCA showed good agreement with the results obtained using conventional biological assays, such as viability, TUNEL, and western blot assays, as described in the previous section. Thus, this technique can be used to assess the apoptotic effect of BV using a noninvasive, label-free quality assessment of the cellular changes.

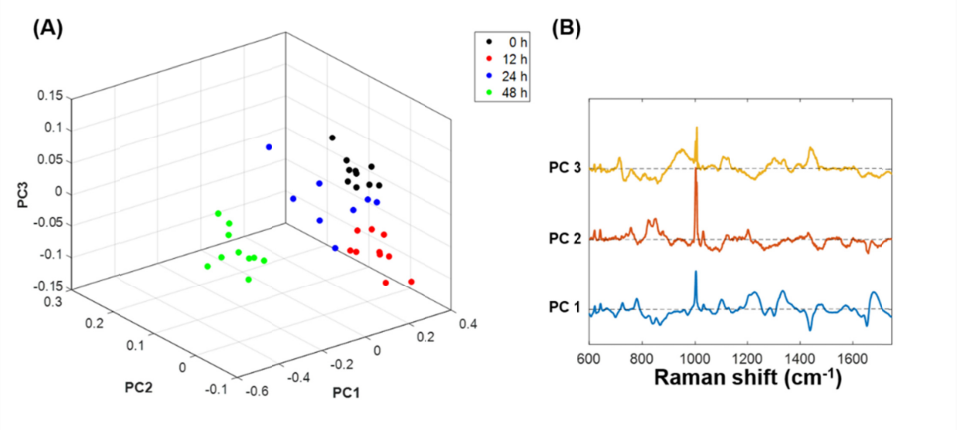

Fig. 7. Score plot and Loading plot for the Raman spectral data at the selected time points. (A) Score plot reveals the projection of the data onto the PCs in three dimensions for the Raman spectral data. (B) Loading plot highlights the important frequencies which contribute to each PC for the Raman spectral data.

Biomedical Optics EXPRESS

4. Conclusion

In this study, we demonstrated the effects of concentration- and time-dependent BV treatment using Raman spectroscopy along with multivariate analysis. The Raman spectrum for the cells treated with 3.0 μg/mL of BV for 48 h corresponded to the Raman bands assigned to DNA and protein, and demonstrated a decrease in signal intensity, which was attributed to nuclear fragmentation and protein degradation. Differences in Raman spectra between the control and BV-treated cells correlated with the cellular events during apoptosis. The results of Raman spectroscopy showed good agreement with AFM and the conventional biological assays, such as viability, TUNEL, and western blot assays performed on the same types of cells. This study provides a new method to monitor the concentration- and time-dependent multi-molecular events via measurement of the vibrations of various biomolecules in living cells. Therefore, Raman spectroscopy along with multivariate analysis might be a useful tool for a label-free and noninvasive investigation of the anti-cancer effect of BV on human breast cancer cells.

Funding

National Research Foundation grants funded by the Korean government (MSIP) (No. NRF-2018R1A2B6007635); Basic Science Research Program through the National Research Foundation of Korea (NRF) funded by the Ministry of Education (NRF-2016R1D1A3B03931548).

Disclosures

All authors declare that they have no conflict of interest.

References

1. Y. H. Baek, J. E. Huh, J. D. Lee, D. Y. Choi, and D. S. Park, "Antinociceptive effect and the mechanism of bee venom acupuncture (Apipuncture) on inflammatory pain in the rat model of collagen-induced arthritis: Mediation by alpha2-Adrenoceptors," Brain Res. **1073-1074**, 305–310 (2006).
2. D. J. Son, J. W. Lee, Y. H. Lee, H. S. Song, C. K. Lee, and J. T. Hong, "Therapeutic application of anti-arthritis, pain-releasing, and anti-cancer effects of bee venom and its constituent compounds," Pharmacol. Ther. **115**(2), 246–270 (2007).
3. J. E. Huh, Y. H. Baek, M. H. Lee, D. Y. Choi, D. S. Park, and J. D. Lee, "Bee venom inhibits tumor angiogenesis and metastasis by inhibiting tyrosine phosphorylation of VEGFR-2 in LLC-tumor-bearing mice," Cancer Lett. **292**(1), 98–110 (2010).
4. W. R. Lariviere and R. Melzack, "The bee venom test: a new tonic-pain test," Pain **66**(2-3), 271–277 (1996).
5. R. C. Hider, "Honeybee venom: a rich source of pharmacologically active peptides," Endeavour **12**(2), 60–65 (1988).
6. N. Oršolić, "Bee venom in cancer therapy," Cancer Metastasis Rev. **31**(1-2), 173–194 (2012).
7. M. H. Park, M. S. Choi, D. H. Kwak, K. W. Oh, D. Y. Yoon, S. B. Han, H. S. Song, M. J. Song, and J. T. Hong, "Anti-cancer effect of bee venom in prostate cancer cells through activation of caspase pathway via inactivation of NF-κB," Prostate **71**(8), 801–812 (2011).
8. S. W. Ip, S. S. Liao, S. Y. Lin, J. P. Lin, J. S. Yang, M. L. Lin, G. W. Chen, H. F. Lu, M. W. Lin, S. M. Han, and J. G. Chung, "The role of mitochondria in bee venom-induced apoptosis in human breast cancer MCF7 cells," In Vivo **22**(2), 237–245 (2008).
9. J. H. Park, K. H. Kim, S. J. Kim, W. R. Lee, K. G. Lee, and K. K. Park, "Bee venom protects hepatocytes from tumor necrosis factor-alpha and actinomycin D," Arch. Pharm. Res. **33**(2), 215–223 (2010).
10. H. Hu, D. Chen, Y. Li, and X. Zhang, "Effect of polypeptides in bee venom on growth inhibition and apoptosis induction of the human hepatoma cell line SMMC-7721 *in-vitro* and Balb/c nude mice *in-vivo*," J. Pharm. Pharmacol. **58**(1), 83–89 (2006).
11. T. Putz, R. Ramoner, H. Gander, A. Rahm, G. Bartsch, and M. Thurnher, "Antitumor action and immune activation through cooperation of bee venom secretory phospholipase A_2 and phosphatidylinositol-(3,4)-bisphosphate," Cancer Immunol. Immunother. **55**(11), 1374–1383 (2006).
12. N. A. Thornberry and Y. Lazebnik, "Caspases: enemies within," Science **281**(5381), 1312–1316 (1998).
13. W. C. Earnshaw, L. M. Martins, and S. H. Kaufmann, "Mammalian caspases: structure, activation, substrates, and functions during apoptosis," Annu. Rev. Biochem. **68**(1), 383–424 (1999).
14. A. Strasser, L. O'Connor, and V. M. Dixit, "Apoptosis signaling," Annu. Rev. Biochem. **69**(1), 217–245 (2000).
15. R. A. Nagourney, "Ex vivo programmed cell death and the prediction of response to chemotherapy," Curr. Treat. Options Oncol. **7**(2), 103–110 (2006).

Biomedical Optics EXPRESS

16. J. Lin, R. Chen, S. Feng, J. Pan, B. Li, G. Chen, S. Lin, C. Li, L. Sun, Z. Huang, and H. Zeng, "Surface-enhanced Raman scattering spectroscopy for potential noninvasive nasopharyngeal cancer detection," J. Raman Spectrosc. **43**(4), 497–502 (2012).
17. M. M. Mariani, P. J. Day, and V. Deckert, "Applications of modern micro-Raman spectroscopy for cell analyses," Integr. Biol. **2**(2-3), 94–101 (2010).
18. S. Dochow, C. Krafft, U. Neugebauer, T. Bocklitz, T. Henkel, G. Mayer, J. Albert, and J. Popp, "Tumour cell identification by means of Raman spectroscopy in combination with optical traps and microfluidic environments," Lab Chip **11**(8), 1484–1490 (2011).
19. G. B. Jung, Y. J. Lee, G. Lee, and H. K. Park, "A simple and rapid detection of tissue adhesive-induced biochemical changes in cells and DNA using Raman spectroscopy," Biomed. Opt. Express **4**(11), 2673–2682 (2013).
20. S. Feng, R. Chen, J. Lin, J. Pan, Y. Wu, Y. Li, J. Chen, and H. Zeng, "Gastric cancer detection based on blood plasma surface-enhanced Raman spectroscopy excited by polarized laser light," Biosens. Bioelectron. **26**(7), 3167–3174 (2011).
21. P. N. Goel, S. P. Shigh, C. Murali Krishna, and R. P. Gude, "Investigating the effects of Pentoxifylline on human breast cancer cells using Raman spectroscopy," J. Innov. Opt. Health Sci. **8**(2), 1550004 (2015).
22. I. Notingher, J. Selvakumaran, and L. L. Hench, "New detection system for toxic agents based on continuous spectroscopic monitoring of living cells," Biosens. Bioelectron. **20**(4), 780–789 (2004).
23. E. Brauchle, S. Thude, S. Y. Brucker, and K. Schenke-Layland, "Cell death stages in single apoptotic and necrotic cells monitored by Raman microspectroscopy," Sci. Rep. **4**(1), 4698 (2015).
24. R. Buckmaster, F. Asphahani, M. Thein, J. Xu, and M. Zhang, "Detection of drug-induced cellular changes using confocal Raman spectroscopy on patterned single-cell biosensors," Analyst (Lond.) **134**(7), 1440–1446 (2009).
25. H. Yao, Z. Tao, M. Ai, L. Peng, G. Wang, B. He, and Y. Li, "Raman spectroscopic analysis of apoptosis of single human gastric cancer cells," Vib. Spectrosc. **50**(2), 193–197 (2009).
26. C. A. Owen, J. Selvakumaran, I. Notingher, G. Jell, L. L. Hench, and M. M. Stevens, "In vitro toxicology evaluation of pharmaceuticals using Raman micro-spectroscopy," J. Cell. Biochem. **99**(1), 178–186 (2006).
27. T. J. Moritz, D. S. Taylor, D. M. Krol, J. Fritch, and J. W. Chan, "Detection of doxorubicin-induced apoptosis of leukemic T-lymphocytes by laser tweezers Raman spectroscopy," Biomed. Opt. Express **1**(4), 1138–1147 (2010).
28. A. Zoladek, F. C. Pascut, P. Patel, and I. Notingher, "Non-invasive time-course imaging of apoptotic cells by confocal Raman micro-spectroscopy," J. Raman Spectrosc. **42**(3), 251–258 (2011).
29. B. Kang, L. A. Austin, and M. A. El-Sayed, "Observing real-time molecular event dynamics of apoptosis in living cancer cells using nuclear-targeted plasmonically enhanced Raman nanoprobes," ACS Nano **8**(5), 4883–4892 (2014).
30. Z. Farhane, F. Bonnier, and H. J. Byrne, "An in vitro study of the interaction of the chemotherapeutic drug Actinomycin D with lung cancer cell lines using Raman micro-spectroscopy," J. Biophotonics **11**(1), e201700112 (2018).
31. A. Ferrante and Y. H. Thong, "Separation of mononuclear and polymorphonuclear leucocytes from human blood by the one-step Hypaque-Ficoll method is dependent on blood column height," J. Immunol. Methods **48**(1), 81–85 (1982).
32. O. Ernst and T. Zor, "Linearization of the bradford protein assay," J. Vis. Exp. **38**, 1918 (2010).
33. L. Ma, B. Song, H. Jin, J. Pi, L. Liu, J. Jiang, and J. Cai, "Cinobufacini induced MDA-MB-231 cell apoptosis-associated cell cycle arrest and cytoskeleton function," Bioorg. Med. Chem. Lett. **22**(3), 1459–1463 (2012).
34. Y. J. Lee, G. J. Lee, S. W. Kang, Y. Cheong, and H. K. Park, "Label-free and quantitative evaluation of cytotoxicity based on surface nanostructure and biophysical property of cells utilizing AFM," Micron **49**, 54–59 (2013).
35. Q. Matthews, A. Jirasek, J. Lum, X. Duan, and A. G. Brolo, "Variability in Raman spectra of single human tumor cells cultured in vitro: correlation with cell cycle and culture confluency," Appl. Spectrosc. **64**(8), 871–887 (2010).
36. J. W. Chan, D. S. Taylor, T. Zwerdling, S. M. Lane, K. Ihara, and T. Huser, "Micro-Raman spectroscopy detects individual neoplastic and normal hematopoietic cells," Biophys. J. **90**(2), 648–656 (2006).
37. I. Notingher, J. Selvakumaran, and L. L. Hench, "New detection system for toxic agents based on continuous spectroscopic monitoring of living cells," Biosens. Bioelectron. **20**(4), 780–789 (2004).
38. A. B. Veloso, J. P. F. Longo, L. A. Muehlmann, B. F. Tollstadius, P. E. N. Souza, R. B. Azevedo, P. C. Morais, and S. W. da Silva, "SERS Investigation of Cancer Cells Treated with PDT: Quantification of Cell Survival and Follow-up," Sci. Rep. **7**(1), 7175 (2017).
39. L. A. Muehlmann, M. C. Rodrigues, J. P. Longo, M. P. Garcia, K. R. Py-Daniel, A. B. Veloso, P. E. de Souza, S. W. da Silva, and R. B. Azevedo, "Aluminium-phthalocyanine chloride nanoemulsions for anticancer photodynamic therapy: Development and in vitro activity against monolayers and spheroids of human mammary adenocarcinoma MCF-7 cells," J. Nanobiotechnology **13**(1), 36 (2015).
40. J. Zhu, J. Zhou, J. Guo, W. Cai, B. Liu, Z. Wang, and Z. Sun, "Surface-enhanced Raman spectroscopy investigation on human breast cancer cells," Chem. Cent. J. **7**(1), 37 (2013).
41. L. Su, Y. Chen, G. N. Zhang, L. H. Wang, A. G. Shen, X. D. Zhou, X. H. Wang, and J. M. Hu, "In vivo and in situ monitoring of the nitric oxide stimulus response of single cancer cells by Raman spectroscopy," Laser Phys.

Biomedical Optics EXPRESS

Lett. **10**(4), 045608 (2013).
42. I. Notingher, C. Green, C. Dyer, E. Perkins, N. Hopkins, C. Lindsay, and L. L. Hench, "Discrimination between ricin and sulphur mustard toxicity in vitro using Raman spectroscopy," J. R. Soc. Interface **1**(1), 79–90 (2004).
43. J. Dong, Z. L. Wan, Y. C. Chu, S. N. Nakagawa, P. G. Katsoyannis, M. A. Weiss, and P. R. Carey, "Isotope-edited Raman spectroscopy of proteins: a general strategy to probe individual peptide bonds with application to insulin," J. Am. Chem. Soc. **123**(32), 7919–7920 (2001).
44. A. Ianoul, M. N. Boyden, and S. A. Asher, "Dependence of the peptide amide III vibration on the phi dihedral angle," J. Am. Chem. Soc. **123**(30), 7433–7434 (2001).
45. S. A. Asher, A. Ianoul, G. Mix, M. N. Boyden, A. Karnoup, M. Diem, and R. Schweitzer-Stenner, "Dihedral psi angle dependence of the amide III vibration: a uniquely sensitive UV resonance Raman secondary structural probe," J. Am. Chem. Soc. **123**(47), 11775–11781 (2001).
46. A. M. Herrero, "Raman spectroscopy for monitoring protein structure in muscle food systems," Crit. Rev. Food Sci. Nutr. **48**(6), 512–523 (2008).
47. T. Miura and G. J. Thomas, Jr., "Raman spectroscopy of proteins and their assemblies," Subcell. Biochem. **24**, 55–99 (1995).
48. L. Laporte, J. Stultz, and G. J. Thomas, Jr., "Solution conformations and interactions of alpha and beta subunits of the Oxytricha nova telomere binding protein: investigation by Raman spectroscopy," Biochemistry **36**(26), 8053–8059 (1997).
49. V. A. Iconomidou, D. G. Chryssikos, V. Gionis, M. A. Pavlidis, A. Paipetis, and S. J. Hamodrakas, "Secondary structure of chorion proteins of the teleostean fish Dentex dentex by ATR FT-IR and FT-Raman spectroscopy," J. Struct. Biol. **132**(2), 112–122 (2000).
50. A. Torreggiani, G. Bottura, and G. Fini, "Interaction of biotin and biotinyl derivatives with avidin: conformational changes upon binding," J. Raman Spectrosc. **31**(5), 445–450 (2000).
51. A. Torreggiani and A. Tinti, "Raman spectroscopy a promising technique for investigations of metallothioneins," Metallomics **2**(4), 246–260 (2010).
52. C. Ferraro-Peyret, L. Quemeneur, M. Flacher, J. P. Revillard, and L. Genestier, "Caspase-independent phosphatidylserine exposure during apoptosis of primary T lymphocytes," J. Immunol. **169**(9), 4805–4810 (2002).
53. M. L. Coleman, E. A. Sahai, M. Yeo, M. Bosch, A. Dewar, and M. F. Olson, "Membrane blebbing during apoptosis results from caspase-mediated activation of ROCK I," Nat. Cell Biol. **3**(4), 339–345 (2001).